Nanoscale

Accepted Manuscript

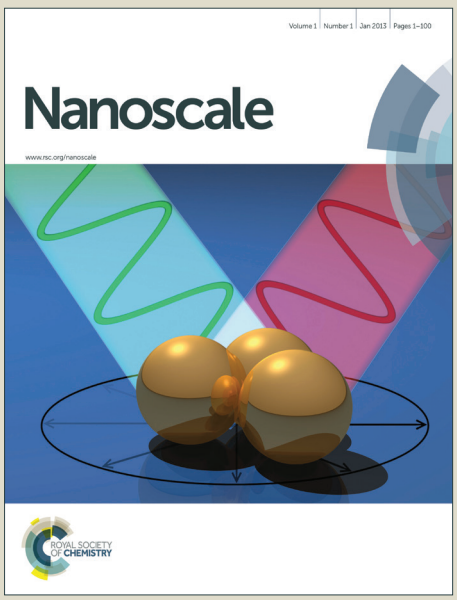

ROYAL SOCIETY OF CHEMISTRY

www.rsc.org/nanoscale

Nanoscale

RSCPublishing

ARTICLE

Polarization Enhancement of Microwave Absorption by Increasing Aspect Ratio of Ellipsoidal Nanorattles with Fe_3O_4 Cores and Hierarchical $CuSiO_3$ Shells

Cite this: DOI: 10.1039/x0xx00000x

Junjie Xu[#,†], Jiwei Liu[#,†,§], Renchao Che[*,†], Chongyun Liang[†], Maosheng Cao[‡], Yong Li[‡], Zhengwang Liu[†]

Received
Accepted

DOI: 10.1039/x0xx00000x

www.rsc.org/

The shape anisotropy of the nanostructured nanorattles is one of the key factors that affect their microwave absorption performance. In the present work, the microwave absorption performance of ellipsoidal Fe_3O_4@$CuSiO_3$ nanorattles with different aspect ratio was investigated. Results demonstrated that the ellipsoidal nanorattles with the aspect ratio of 3-4 exhibited about 20% enhancement of microwave absorption intensity compared with spherical Fe_3O_4@$CuSiO_3$. Generally, as the aspect ratio increased from 2.0 to 3.5, the microwave absorption peak was enhanced monotonously from -20 dB to -30 dB. It was found that the ellipsoidal nanorattles with larger aspect ratio exhibited higher coercivity and double resonance peaks of the real part of complex permittivity, resulting in the improvement of microwave absorption performance. Our research gives insights into the understanding of the anisotropic effect of nanorattles on microwave absorption performance.

Introduction

With the rapid increase in the requirement of electronic apparatus, the research of high-efficient microwave absorber against electromagnetic interference (EMI) has become a great concern. During the past decades, a lot of efforts have been devoted to designing a variety of materials and structures used as microwave absorbers for stealth and shielding applications.[1-6] Magnetite (Fe_3O_4) has been attracting extensive interest as microwave absorption agent because of the merits of low cost and strong magnetic absorption.[7, 8] However, magnetite suffers from the shortcomings of ease oxidation, high density and narrow absorption frequency band, which hamper its practical applications.

Nowadays, core/shell or yolk/shell structure with Fe_3O_4 as a core has been applied in many fields including nanoreactors, catalysis and biomedical fields because of its unique properties resulted from the synergistic effects of both the cores and shells,[6, 9, 10] based on which, core/shell or yolk/shell structures have been previously reported as a promising candidate for microwave absorber due to its advantages: light weight and wide absorption band. Moreover, the shell could protect the Fe_3O_4 core from environmental oxidation.[5, 11]

Recently, our group has reported the microwave absorption property of rattle-type microspheres with Fe_3O_4 core and hierarchical silicate copper shell which exhibit a maximum absorption intensity of -25dB and a frequency range of 8GHz below -10dB.[12] The enhanced absorption capability could be ascribed to the unique hierarchical structure with complicate geometrical morphologies leading to strong interface scattering and polarization loss.[13] Besides the hierarchical structure contributed from core-shell and yolk-shell structure, Sun et al have reported strong performance of microwave absorption of hierarchical dendrite-like Fe_3O_4, γ-Fe_2O_3, and Fe.[14] In most cases, the resulting rattle-type hierarchical structures are spherical in shape. However, previous reports on nonspherical microwave absorber made up of rattle-type yolk-shell structure are still scarce.[15] Furthermore, the anisotropic rattle-type structure has rarely been systematically studied from the perspective of the correlations between microwave absorption performance and structural factors: aspect ratio, size of the core, and the thickness of the shell of the nanoparticles.

On the other hand, reports shows that the aspect ratio and size have significant impact on the absorption properities.[4] Considering the effects of shape anisotropy, especially the dependence of microwave absorption on aspect ratio and size, many experimental and theoretical efforts have been reported. For example, reports show that one-dimensional carbon nanotube polymer composites,[16-18] plait-like carbon nanocoils,[19] and ZnO dendritic structure[20] with higher aspect ratio value exhibit better absorption performance than nanoparticles due to

[†]Department of Materials Science and Laboratory of Advanced Materials, Fudan University, Shanghai 200438, China, rcche@fudan.edu.cn
[‡]School of Materials Science and Engineering, Beijing Institute of Technology, Beijing 100081, China,
[§]National Institute for Materials Science (NIMS), Sengen 1-2-1, Tsukuba, Ibaraki 305-0047, Japan
[#]These authors contributed equally

the higher image part of the complex permitivity.[21] Recently, there are corresponding results about magnetic materials, such as Fe–Cr–Si–Al alloy flakes,[22] $Fe_{55}Ni_{45}$,[23] barium ferrite nanorods.[24] These results show that the intensity of reflection loss (RL) significantly increases with the enlarging aspect ratio due to a higher resonance frequency over the Snock's limit in the gigahertz frequency range resulting from lower eddy current loss.[25, 26] The shape anisotropy endows the soft magnetic materials an ability of overcoming the difficulty of comparatively small intrinsic anisotropy and increasing the natural resonant frequencies to the gigahertz range, leading to higher real and imaginary part of the permeability.[26, 27]

However, the influence of aspect ratio and size on the combined dielectric–magnetic materials has not been invested till now as far as we know. And this effect is of importance for dielectric-magnetic materials with hierarchical structure because the interface between dielectric and magnetic materials contributes to the permittivity and permeability of the system while the microwave absorption performance is determined by the match of the permittivity and permeability rather than their absolute value.

Herein, we report that increasing the aspect ratio could enhance the microwave absorption performance of ellipsoidal nanorattles with magnetic Fe_3O_4 cores and hierarchical copper silicate shells (denoted as Fe_3O_4@CuSilicate) because of the improvement of coercivity and dielectric loss. Compared with the spherical Fe_3O_4@CuSilicate nanoparticles with yolk-shell structure, the ellipsoidal nanorattles with the aspect ratio of 3-4 showed about 20% microwave absorption intensity enhancement. Moreover, the match of magnetic loss and dielectric loss is beneficial for the improvement of microwave absorption of the Fe_3O_4@CuSilicate system.

Results and discussion

The synthesis procedure consists of three main steps (Scheme 1). Firstly, to obtain core-shell nanospindles (designated as α-Fe_2O_3@SiO_2) uniform α-Fe_2O_3 nanospindles are coated with silica via the Stöber method.[28] Secondly, the obtained α-Fe_2O_3@SiO_2 nanospindles are hydrothermally treated in aqueous $Cu(NO_3)_2$ and ammonia solution at 120 ℃, leading to the formation of ellipsoidal nanorattles with α-Fe_2O_3 cores and hierarchical copper silicate shells (designated as α-Fe_2O_3@CuSilicate).[29] Thirdly, the resulting α-Fe_2O_3@CuSilicate nanorattles are reduced in H_2/N_2 atmosphere to obtain the ellipsoidal nanorattles with magnetic Fe_3O_4 cores and hierarchical copper silicate shells.

Representative TEM images of the uniform α-Fe_2O_3 particles (Fig. 1(a)) shows spindle-like morphology and the size of approximately ~608 nm in length and ~132 nm in width. FESEM image (Fig. 1(b)) reveals that the α-Fe_2O_3 nanospindles with very rough surface are actually composed of small primary nanocrystals. By using the Stöber method, the α-Fe_2O_3 nanospindles can be easily coated with a silica layer of ~60 nm in thickness (Fig. 1(c)). It can be clearly seen in Fig. 1(d) that the as-made α-Fe_2O_3@SiO_2 nanospindles show a relatively smooth surface due to the deposition and growth of the silica layer. Moreover, the thickness of the silica layers can be readily controlled by tuning the concentrations of α-Fe_2O_3. For example, when the α-Fe_2O_3 concentration increases from 0.2 to 0.4 g L^{-1}, the thickness of the silica layers for the α-Fe_2O_3@SiO_2 nanospindles can be varied from ~60 to ~27 nm (Electronic Supplementary Material, Fig. S 1).

The size and morphology of the as-synthesized α-Fe_2O_3@CuSilicate nanorattles are characterized using the FESEM. SEM image of the as-made α-Fe_2O_3@Cusilicate nanorattles in Fig. 1(e) demonstrates the urchin-like structure and nearly monodispersed characteristic with an aspect ratio of 2~3. The unique rattle-type structure is clearly revealed by the TEM image in Fig. 1(f), from which a dark particle with an aspect ratio of 4~5 individually encapsulated in hierarchical shells of ~60 nm in thickness can be observed. The nanorattles duplicate the ellipsoidal morphology of the α-Fe_2O_3 templates and the shell is assembled by a large number of nanosheets, which is consistent with the SEM observation. EDS analysis of the as-synthesized nanorattles indicates the presence of Fe, O, Cu, and Si elements in the nanorattles (Electronic Supplementary Material, Fig. S 2). To further investigate their microstructure, BF/HAADF-STEM imaging is employed. The corresponding elemental mappings shown in Fig. 1(g)-(k) demonstrate (g) RGB cropped image of an individual α-Fe_2O_3@CuSilicate nanorattle and corresponding elemental mapping: (h) Fe, (i) O, (j) Cu, (k) Si elements in the nanorattle. Iron can be clearly seen in the core region (Fig. 1(h)) and the Cu and Si can be detected from the shell region (Fig. 1(j) and (k)), while the O can be detected in both the core and shell regions (Fig. 1(i)). Moreover, as shown in Fig. 1(h)-(j), BF/HAADF-STEM images of an individual nanorattle combined with line scanning profiles further confirm that the component of α-Fe_2O_3 located in the core is surrounded by the hierarchical copper silicate shells. From the SEM, TEM, and BF/HAADF-STEM results, it can be confirmed that the α-Fe_2O_3@Cusilicate nanorattles with ellipsoidal α-Fe_2O_3 cores and hierarchical copper silicate shells have been successfully synthesized.

After the annealing treatment at 450 ℃ in H_2/N_2 (5% H_2) atmosphere, the ellipsoidal structure of the nanorattles has been well-retained (Fig. 2(a)). It can be clearly seen in Fig. 2(b) and (c) that there is no significant change in morphology, indicating that the hierarchical copper silicate shells keep unchanged during the reduction process. Furthermore, the cores still exhibit regular ellipsoidal shape despite the change of structure in the transformation from α-Fe_2O_3 to Fe_3O_4. The corresponding HRTEM image (Fig. 2(d)) and SAED pattern (Fig. 2(e)) recorded on the edge of the nanorattle indicate that the shell is of high crystallinity. It can be found in Fig. 2(d) that there is interplanar spacing of ~0.26 nm, which correspond to the (312) of copper silicate (JCPDS card no. 32-0346).

The crystal structure and phase purity of the as-synthesized products are identified by XRD. Fig. 2(f) shows the typical XRD pattern of the α-Fe_2O_3. All apparent diffraction peaks can be assigned to hematite (JCPDS card no. 33-0664). After coating with the SiO_2 layer, no characteristic peaks of other materials can be detected, indicating the SiO_2 is amorphous (Fig. 2(g)). Fig. 2(h) shows the XRD pattern of the α-Fe_2O_3@CuSilicate nanorattles. As can be seen, there is no characteristic peaks of copper silicate, thereby indicating that the hydrothermally synthesized copper silicate shells are poorly crystalline. After reduction by H_2 at 450 °C for 2h, XRD pattern of the Fe_3O_4@CuSilicate nanorattles (Fig. 2(i)) shows new characteristic diffraction peaks, which can be indexed to magnetite (JCPDS card no. 19-0629) and copper silicate (JCPDS card no. 32-0346), respectively. Combined with XPS spectra of Fe_3O_4@CuSilicate nanorattles (Electronic Supplementary Material, Fig. S 4) and mixture of Fe_3O_4 and copper silicate (Electronic Supplementary Material, Fig. S 5), the XRD patterns demonstrate the successful transformation

from α-Fe_2O_3 to Fe_3O_4 and high crystallinity and phase purity of the copper silicate shells, which agree well with the HRTEM and SAED results.

In this work, the thicknesses of the copper silicate shells of these nanorattles can be readily tailored by changing the thicknesses of SiO_2 layer. Fig. 3(b) shows the TEM image of the α-Fe_3O_4@CuSilicate nanorattles (denoted as MCS-1) with the aspect ratio of ~2.3 using the α-Fe_2O_3@SiO_2 with ~68 nm SiO_2 layer thickness as the templates, following the step of reduction with H_2. It can be seen that the thickness of the copper silicate shells for the resulting nanorattles is ~70 nm. When using the α-Fe_2O_3@SiO_2 with the SiO_2 thickness of ~95 nm as the templates and keeping other experimental parameters unchanged, the shell thickness of the copper silicate shells for the resulting α-Fe_3O_4@CuSilicate nanorattles (denoted as MCS-2) increases to ~100 nm (Fig. 3(c)). These results indicate that the SiO_2 layer actually act not only as a sacrificial template for the hollow structure but also as the origin materials for the formation of copper silicate shells.[9, 30] Similarly, using the α-Fe_2O_3@SiO_2 with the aspect ratio of 4~5 as the template, a series of α-Fe_3O_4@CuSilicate nanorattles with the aspect ratio of ~3.5 and the shell thicknesses of ~50 nm (denoted as MCS-3), ~70nm (denoted as MCS-4) and ~110 nm (denoted as MCS-5) have been synthesized by tuning the thickness of the SiO_2 shell, as shown in Fig. 3(d) - (f).

Fig. 4(a) shows hysteresis loop of the Fe_3O_4@CuSilicate nanorattles with different aspecet ratio and shell thickness. As shown in Fig. 4(a), the saturation magnetization (Ms) of the Fe_3O_4@CuSilicate nanorattles decreases with the increasing of the shell thickness when the aspect ratio keeps unchange. However, when the thickness of the silicate copper shell keeps the same, the saturation magnetization (Ms) and the coercivity (Hc) of the Fe_3O_4@CuSilicate nanorattles demonstrate an increasing tendency when the aspect ratio increases. As shown in Fig. 4(b) and Fig. 4(c), with thickness of the silicate copper shell rising and the aspect ratio keeping constant, the coercivity (Hc) increases accordingly. Thus, the Fe_3O_4@CuSilicate nanorattles with larger aspect ratio and shell thickness should lead to materials displaying stronger magnetism[10] which is conducive for magnetic loss of microwave absorber. As shown in Fig. 4(d), the color of the solution changes from brownish-red to black after the reduction process, indicating the successful phase conversion of α-Fe_2O_3 to Fe_3O_4. As a result of the ferromagnetic property and high magnetization, the Fe_3O_4@CuSilicate nanorattles are strongly attracted toward the magnet quickly. After removal of the magnetic field followed by stirring, the aggregations are rapidly re-dispersed. This will allows for an easy and efficient way to separate the nanorattles from a suspension system under an external magnetic field.

To reveal the mechanism of the reflection absorption, dielectric loss factor (tan δ_ε =ε"/ε') and magnetic loss factor (tan δ_m =μ"/μ') are calculated. The value of tan δ_ε and tan δ_m are between 0.1-0.24 and 0.22-0.4, respectively, over the range of 2-12 GHz, as demonstrated in Fig. 6(a). The tan δ_m is larger than tan δ_ε in the whole range, suggesting an evident synergistic absorption effect in this yolk-shell system. The real part of complex permittivity possesses two remarkable resonances peaks (Fig.5b, c), with a value of about 40 or 14 corresponding to different shell thickness. As previously reported,[12] spherical Fe_3O_4@CuSilicate does not exhibit similar double resonance peaks, strongly indicting a unique dielectric loss phenomena contributed from ellipsoidal nanorattles morphology. It is supposed that ellipsoidal nanorattles with hierarchical structure generate strong dielectric polarization loss.[14, 31] As calculated by the BET method, such a rattle-type structure gives rise to BET surface area of 137 m^2 g^{-1} and a relatively high pore volume of 0.26 cm^3 g^{-1}, respectively (Electronic Supplementary Material, Fig. S 3). Thus, this electric loss could be resulted from large specific surface (amounts of primiary-unit nanoparticles), interface polarization, morphology dielectric polarization (anisotropy shape).[32-34]

It is well-known that the microwave absorption properties of a material are closely related to the aspect ratio and geometry parameter of the absorber.[4, 32] Very recently, our group have demonstrated the synthesis of spherical magnetic rattle-type microspheres with Fe_3O_4 cores and hierarchical silicate copper shells for microwave absorption enhancement.[12] In this study, the combination of the magnetic Fe_3O_4 core and hierarchical copper silicate shells, in addition to hollow ellipsoidal morphology, is important for the as-synthesized ellipsoidal Fe_3O_4@CuSilicate nanorattles to be used in microwave absorption. The microwave absorption properties of the ellipsoidal Fe_3O_4@CuSilicate nanorattles are investigated in terms of reflection loss. The reflection loss (RL) values are calculated using the relative complex permittivity and permeability at a given frequency and thickness layer according to the transmit line theory, which is summarized as the following equations:[35, 36]

$$Z_{in} = \sqrt{\mu_r / \varepsilon_r}\tanh[-j(2\pi fd/c)\sqrt{\mu_r/\varepsilon_r}]$$

$$RL(dB) = -20\log_{10}\left|(Z_{in}-1)/(Z_{in}+1)\right|$$

where ε_r and μ_r are the relative complex permittivity and permeability of the absorber medium, f is the frequency of microwave in free space, c is the velocity of light, d is the coating thickness, and Z_{in} is the input impedance of the absorber.

Fig. 6 shows the RL data for the α-Fe_2O_3/EP, α-Fe_2O_3@SiO_2/EP, α-Fe_2O_3@CuSilicate/EP and all Fe_3O_4@CuSilicate/EP composites with the measured film thickness d=2, 2.5, 3, 3.5, 4mm, respectively. The value of maximum RL of the α-Fe_2O_3 and spindle-like Fe_3O_4 nanoparticles, for example, at d= 2 mm, are -4 dB at 10 GHz and -14dB at 3GHz frequency range (Fig. 6(b)), while the α-Fe_2O_3@SiO_2 shows maximum RL value of -3.8 dB with the same thickness. A maximum RL value of -8 dB at 18 GHz is obtained from the α-Fe_2O_3@CuSilicate. As expected, the Fe_3O_4@CuSilicate nanorattles display significantly enhanced microwave absorption properties compared to the α-Fe_2O_3 nanospindles, spindle-like Fe_3O_4 nanoparticles and the α-Fe_2O_3@CuSilicate nanorattles, in terms of both the maximum RL value and the absorption bandwidth. It can be seen in Fig. 6(b) that the values of maximum RL of the MCS-1, MCS-4, and MCS-5 are -12, -21.3 and -30.8 dB with a thickness of 2 mm, respectively. While, RL value of the random mixture of Fe_3O_4 and copper silicate is -10dB, suggesting that the structure of rattle type contributes a lot to the strong microwave absorption of Fe_3O_4@CuSilicate nanorattles. Besides the geometrical absorption/scattering effect,[4, 32] large specific surface area[33, 34] and the void space existing between core and shell as we mentioned in our former paper,[12] the effect of the thickness of shell and the aspect ratio play an important role in this system. When the shell thickness keeps unchanged, the intensity of absorption tends to increase with the rising of aspect ratio. (Electronic Supplementary Material, Fig. S 6) Moreover, the shell thickness is beneficial for the microwave absorption. (Electronic Supplementary Material, Fig. S 7) This

tendency is also remarkable when the measured film d= 2.5, 3, 3.5, 4mm, as shown in Fig. 6(c)-(f).

On the basis of the above discussion, the excellent microwave absorption performance may be attributed to the unique structure of the Fe_3O_4@CuSilicate nanorattles. As shown in Fig. 7, the mechanism of enhanced microwave absorption could be ascribed to the following points. Firstly, the higher coercivity and larger $(BH)_{max}$ resulting from shape anisotropy and magnetocrystalline[37] are beneficial for strong microwave absorption through magnetic loss. Secondly, the high-curvature surfaces will lead to more remarkable interface polarization compared with spherical nanoparticles with similar composition and structure. For elliptical nanoparticles, their high-curvature surfaces will cause more dangling bonded atoms and unsaturated coordination on the surface of nanoparticles, which may lead to more remarkable interface polarization compared with spherical nanoparticles.[38] Thirdly, the effective complementarities between the magnetic loss and the dielectric loss, which originate from the synergistic effect of the Fe_3O_4 cores and copper silicate shells, endow this system a wide absorption band.[13, 28] Because of its relatively low tan δ_ε and high tan δ_μ values, the EM impedance matching is more fulfilled in the Fe_3O_4@CuSilicate nanorattles with thicker copper silicate shells, which are responsible for the significantly enhanced microwave absorption properties.[39] These results highlight the importance of a unique rattle-type structure and are helpful for a better understanding of the effect of aspect ratio and shell size on the performance of microwave absorber.

Conclusions

In summary, this study shows that the ellipsoidal Fe_3O_4@CuSilicate nanorattles exhibited enhanced microwave absorption performance compared with spherical Fe_3O_4@CuSilicate nanorattles because of the strong magnetic loss and the improvement of dielectric loss. This could be corroborated by the enlargement of coercivity and the apparent double resonance peaks of the real part of complex permittivity which leads to the enhancement of interface polarization. These results could be further confirmed by the hysteresis loop, frequency dependence of complex permittivity and permeability of ellipsoidal Fe_3O_4@CuSilicate nanorattles. More interestingly, we have found that enhanced microwave absorption was achieved by regulating the aspect ratio due to the synergistic effect of the core and shell of Fe_3O_4@CuSilicate nanorattles and the match of magnetic loss and dielectric loss. By increasing the aspect ratio from 2.3 to 4.5, enhancement of -18dB is achieved. Such understanding on the influence of aspect ratio will be shown to be very useful for the improvement of microwave absorption performance.

Materials and method

Materials. Ferric chloride hexahydrate ($FeCl_3 \cdot 6H_2O$), sodium dihydrogen phosphate ($NaH_2PO_4 \cdot 2H_2O$), copper nitrate ($Cu(NO_3)_2 \cdot 3H_2O$), tetraethyl orthosilicate (TEOS), ethanol, isopropanol and ammonia solution (28 wt%) were all purchased from Shanghai Sinopharm Chemical Reagent Co., Ltd. All chemicals were of analytical grade and used without further purification. Deionized water obtained from Milli-Q system (Millipore, Bedford, MA) was used in all experiments.

Preparation of α-Fe_2O_3 nanospindles. Uniform spindle-like α-Fe_2O_3 nanoparticles were prepared by hydrothermal method as reported previously.[40] Briefly, a 160 mL aqueous solution containing 20 mM $FeCl_3$ and 0.4 mM NaH_2PO_4 was transferred into a Teflon-lined stainless-steel autoclave with a capacity of 200 mL. The autoclave was maintained at 105 ^oC for 50 h, and then allowed to cool to room temperature. The obtained α-Fe_2O_3 nanospindles were centrifuged and thoroughly rinsed with ethanol and water several times, and dried at 60 ^oC for 12 h.

Synthesis of α-Fe_2O_3@SiO_2 nanospindles. The core-shell α-Fe_2O_3@SiO_2 nanospindles were synthesized through a modified Stöber method.[28] For a typical procedure, 0.015 g of the as-prepared α-Fe_2O_3 nanospindles were dispersed in a mixture of 65 mL of isopropanol, 6.5 mL of water, and 0.6 mL of ammonia solution. Afterward, 0.3 mL of TEOS was added dropwise, and stirred for 8 h at room temperature. The as-made α-Fe_2O_3@SiO_2 nanospindles were centrifuged and rinsed with ethanol for four times, and dried at 60 ^oC for 12 h.

Synthesis of α-Fe_2O_3@CuSilicate nanorattles. The α-Fe_2O_3@CuSilicate nanorattles were synthesized with the previously reported method.[41] Briefly, 0.02 g of the α-Fe_2O_3@SiO_2 nanospindles were dispersed in water (36 mL) by ultrasonication for 20 min, then 2 mL of ammonia solution was added under stirring. After stirring for 5 min, an aqueous $Cu(NO_3)_2$ solution (1.2 mL, 0.1 M) was added dropwise and stirred for another 5 min. Then, the mixed solution was transferred into a Teflon-lined stainless-steel autoclave (50 mL). The autoclave was heated at 120 ^oC for 12 h, and then allowed to cool to room temperature. The final products were centrifuged and rinsed with ethanol several times, and dried at 60 ^oC for 12 h.

Synthesis of Fe_3O_4@CuSilicate nanorattles. The Fe_3O_4@Cusilicate nanorattles were obtained by reducing the as-synthesized α-Fe_2O_3@Cusilicate nanorattles in a furnace under a flowing H_2/N_2 (5% H_2) atmosphere at 450 ^oC for 2 h.

Characterization. Transmission electron microscopy (TEM) images, high-resolution TEM (HRTEM), bright-field and high angle annular dark-field scanning transmission electron microscopy (BF/HAADF-STEM) images, energy dispersive X-ray spectroscopy (EDS), and selected-area electron diffraction poatterns (SAED) were acquired using a JEOL JEM-2100F transmission electron microscope equipped with a post-column Gatan imaging filter (GIF-Tridium) at an acceleration voltage of 200 kV. Field-emission scanning electron microscopy (FESEM) imaging were carried out via a Hitachi S-4800 field-emission scanning electron microscope operated at 1.0 kV. Powder X-ray diffraction (XRD) measurements were performed using a Bruker D8 X-ray diffractometer with Ni-filtered Cu K_α radiation (40 kV, 40 mA). Magnetic properties were determined with superconducting quantum interference device (MPMS(SQUID)VSM) magnetometer (Quantum Design Company). Nitrogen adsorption isotherms measurement was carried out at 77 K with a Micromeritics Tristar 3020 analyzer. The Brunauer–Emmett–Teller (BET) method was used to calculate the specific surface areas utilizing adsorption data in a relative pressure from 0.05 to 0.25.

Electromagnetic measurements. Microwave absorption properties were studied by dispersing the samples into epoxy resin (EP) with a weight ratio of 1:5 according to the optimized proportion (Electronic Supplementary Material, Fig. S 8).[5] A portion of the composite was coated on an aluminum substrate (180 mm × 180 mm) with a thickness of 2 mm to measure the

reflection loss of the samples. The remaining sample was molded into the hollow pipe of a rectangular wave guide cavity with dimensions of 10.2 mm × 2.9 mm × 1.2 mm for complex permittivity and permeability measurements. The complex relative permittivity, permeability, and reflection loss were measured with a HP8510C vector network analyzer in the 2-18 GHz range.

Acknowledgements

This work was supported by the Ministry of Science and Technology of China (973 Project Nos. 2013CB932901 and 2009CB930803), and the National Natural Foundation of China (Nos. 51172047, 50872145, 51102050 and U1330118). This project was sponsored by Shanghai Pujiang Program and "Shu Guang" project of Shanghai Municipal Education Commission and Shanghai Education Development Foundation (09SG01).

Electronic Supplementary Material: Supplementary material (details of the TEM imaging, EDS pattern, N_2 adsorption-desorption isotherms, reflection loss of Fe_3O_4@Cu silicate nanorattles with different aspect ratio and shell thickness, XPS spectra of Fe_3O_4@Cu silicate nanorattles) is available free of charge via the Internet at http://pubs.rsc.org.

Notes and references

1. C. Wang, X. Han, P. Xu, J. Wang, Y. Du, X. Wang, W. Qin and T. Zhang, *J. Phys. Chem. C*, 2010, 114, 3196.
2. A. Ghasemi and A. Morisako, J. Magn. Magn. Mater., 2008, 320, 1167.
3. Z. H. Wang, Z. Han, D. Y. Geng and Z. D. Zhang, *Chem. Phys. Lett.*, 2010, 489, 187.
4. H. Li, Y. Huang, G. Sun, X. Yan, Y. Yang, J. Wang and Y. Zhang, *J. Phys. Chem. C*, 2010, 114, 10088.
5. J. Liu, R. Che, H. Chen, F. Zhang, F. Xia, Q. Wu and M. Wang, *Small*, 2012, 8, 1214.
6. S. J. Yan, L. Zhen, C. Y. Xu, J. T. Jiang, W. Z. Shao and J. K. Tang, *J. Magn. Magn. Mater.*, 2011, 323, 515.
7. X. Li, B. Zhang, C. Ju, X. Han, Y. Du and P. Xu, *J. Phys. Chem. C*, 2011, 115, 12350.
8. F. Wang, J. Liu, J. Kong, Z. Zhang, X. Wang, M. Itoh and K. Machida, *J. Mater. Chem.*, 2011, 21, 4314.
9. Q. Fang, S. Xuan, W. Jiang and X. Gong, *Adv. Funct. Mater.*, 2011, 21, 1902.
10. I. Lee, J. B. Joo, Y. Yin and F. Zaera, *Angewandte Chemie*, 2011, 123, 10390.
11. B. Zhang, Y. Du, P. Zhang, H. Zhao, L. Kang, X. Han and P. Xu, *J. Appl. Polym. Sci.*, 2013, 130, 1909.
12. J. Liu, J. Cheng, R. Che, J. Xu, M. Liu and Z. Liu, *ACS Appl. Mater. Interfaces*, 2013, 5, 2503.
13. M. Zhou, X. Zhang, J. Wei, S. Zhao, L. Wang and B. Feng, *J. Phys. Chem. C*, 2010, 115, 1398.
14. G. Sun, B. Dong, M. Cao, B. Wei and C. Hu, *Chem. Mater.*, 2011, 23, 1587.
15. X. W. Lou and L. A. Archer, *Adv. Mater.*, 2008, 20, 1853.
16. N. Li, Y. Huang, F. Du, X. He, X. Lin, H. Gao, Y. Ma, F. Li, Y. Chen and P. C. Eklund, *Nano Letters*, 2006, 6, 1141.
17. Z. Liu, G. Bai, Y. Huang, Y. Ma, F. Du, F. Li, T. Guo and Y. Chen, *Carbon*, 2007, 45, 821.
18. Y. Huang, N. Li, Y. Ma, F. Du, F. Li, X. He, X. Lin, H. Gao and Y. Chen, *Carbon*, 2007, 45, 1614.
19. N. Tang, Y. Yang, K. Lin, W. Zhong, C. Au and Y. Du, *J. Phys. Chem. C*, 2008, 112, 10061.
20. R. F. Zhuo, H. T. Feng, J. T. Chen, D. Yan, J. J. Feng, H. J. Li, B. S. Geng, S. Cheng, X. Y. Xu and P. X. Yan, *J. Phys. Chem. C*, 2008, 112, 11767.
21. R. F. Zhuo, L. Qiao, H. T. Feng, J. T. Chen, D. Yan, Z. G. Wu and P. X. Yan, *J. Appl. Phys.*, 2008, 104, 094101.
22. X. Wang, R. Gong, P. Li, L. Liu and W. Cheng, *Mater. Sci. Eng., A*, 2007, 466, 178.
23. X. Li, R. Gong, Y. Nie, Z. Zhao and H. He, *Mater. Chem. Phys.*, 2005, 94, 408.
24. G. Mu, N. Chen, X. Pan, H. Shen and M. Gu, *Materials Letters*, 2008, 62, 840.
25. R. M. Walser, W. Win and P. M. Valanju, *IEEE Trans. Magn.*, 1998, 34, 1390.
26. R. B. Yang and W. F. Liang, *J. Appl. Phys.*, 2011, 109, DOI: 10.1063/1.3536340.
27. F. Ma, Y. Qin and Y. Z. Li, Appl. Phys. Lett., 2010, 96.
28. J. Liu, J. Xu, R. Che, H. Chen, Z. Liu and F. Xia, *J. Mater. Chem.*, 2012, 22, 9277.
29. T. Zhu, B. Xia, L. Zhou and L. X. Wen, *J. Mater. Chem.*, 2012, 22, 7851.
30. B. T. Zhu, Z. Wang, S. Ding, J. S. Chen and X. W. Lou, *RSC Adv.*, 2011, 1, 397.
31. C. L. Zhu, M. L. Zhang, Y. J. Qiao, G. Xiao, F. Zhang and Y. J. Chen, *J. Phys. Chem. C*, 2010, 114, 16229.
32. X. Qi, Y. Deng, W. Zhong, Y. Yang, C. Qin, C. Au and Y. Du, *J. Phys. Chem. C*, 2009, 114, 808.
33. X. Guo, Y. Deng, D. Gu, R. Che and D. Zhao, *J. Mater. Chem.*, 2009, 19, 6706.
34. Y. Qin, R. Che, C. Liang, J. Zhang and Z. Wen, *J. Mater. Chem.*, 2011, 21, 3960.
35. Y. J. Chen, G. Xiao, T. S. Wang, Q. Y. Ouyang, L. H. Qi, Y. Ma, P. Gao, C. L. Zhu, M. S. Cao and H. B. Jin, *J. Phys. Chem. C*, 2011, 115, 13603.
36. Y. J. Chen, F. Zhang, G. G. Zhao, X. Y. Fang, H. B. Jin, P. Gao, C. L. Zhu, M. S. Cao and G. Xiao, *J. Phys. Chem. C*, 2010, 114, 9239.
37. Y. Soumare, C. Garcia, T. Maurer, G. Chaboussant, F. Ott, F. Fiévet, J. Y. Piquemal and G. Viau, *Adv. Funct. Mater.*, 2009, 19, 1971.
38. K. Singh, A. Ohlan, A. K. Bakhshi and S. K. Dhawan, *Mater. Chem. Phys.*, 2010, 119, 201.
39. Y. J. Chen, P. Gao, R. X. Wang, C. L. Zhu, L. J. Wang, M. S. Cao and H. B. Jin, *J. Phys. Chem. C*, 2009, 113, 10061.
40. M. Ozaki, S. Kratohvil and E. Matijević, *J. Colloid Interface Sci.*, 1984, 102, 146.
41. T. Zhu, B. Xia, L. Zhou and X. Wen Lou, *J. Mater. Chem.*, 2012, 22, 7851.

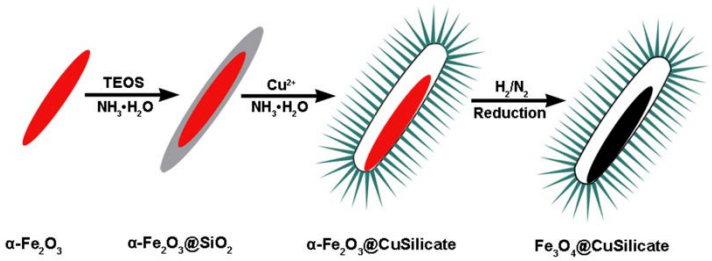

Scheme 1 Schematic illustration of the synthesis procedure for the Fe_3O_4@CuSilicate nanorattles.

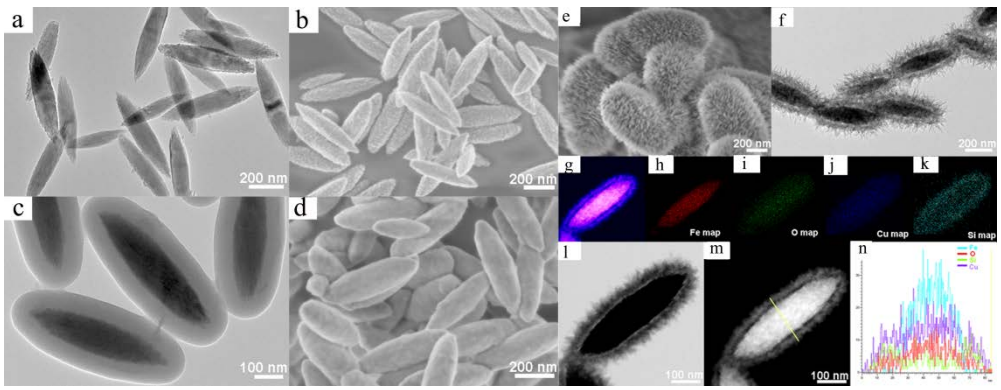

Figure 1 (a) TEM and (b) FESEM images of the α-Fe_2O_3 nano spindles; (c) TEM and (d) FESEM images of the core-shell α-Fe_2O_3@SiO_2 nanospindles, (e) FESEM and (f) TEM images of the α-Fe_2O_3@CuSilicate nanorattles. (g) RGB cropped image of an individual α-Fe_2O_3@CuSilicate nanorattle and corresponding elemental mapping: (h) Fe, (i) O, (j) Cu, (k) Si. (l) BF-STEM image, (m) HAADF-STEM image and (n) line scanning profiles of Fe, O, Si, and Cu recorded along the line of the α-Fe_2O_3@CuSilicate nanorattle in (m).

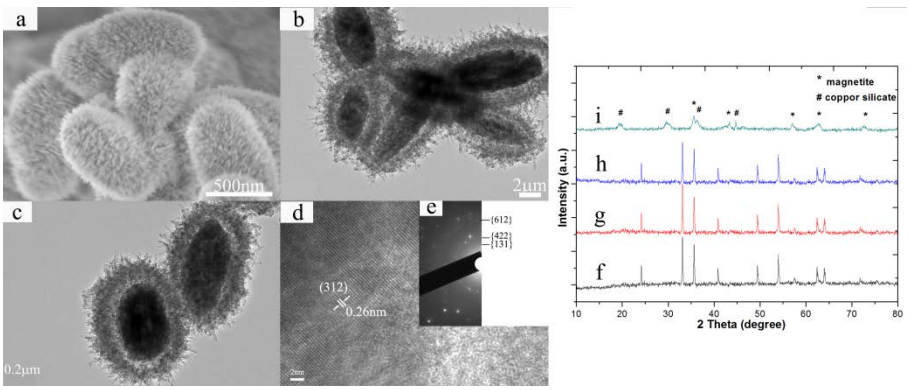

Figure 2 (a) FESEM and (b,c) TEM images of the Fe_3O_4@CuSilicate nanorattles. (d) HRTEM image and (e) SAED pattern taken from the rectangle area in (c). XRD patterns of the (f) α-Fe_2O_3, (g) α-Fe_2O_3@SiO_2, (h) α-Fe_2O_3@CuSilicate, and (i) Fe_3O_4@CuSilicate.

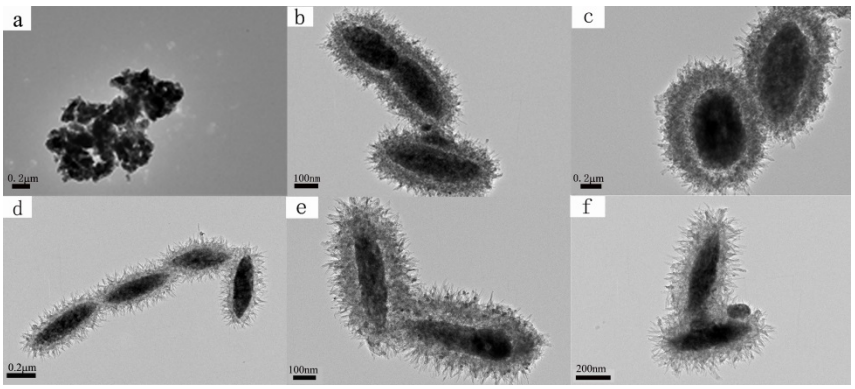

Figure 3 TEM images of (a) the random mixture of Fe_3O_4 and copper silicate, and Fe_3O_4@CuSilicate nanorattles with different aspect ratio and copper silicate shell thicknesses: (b) MCS-1, (c) MCS-2, (d) MCS-3, (e) MCS-4, and (f) MCS-5.

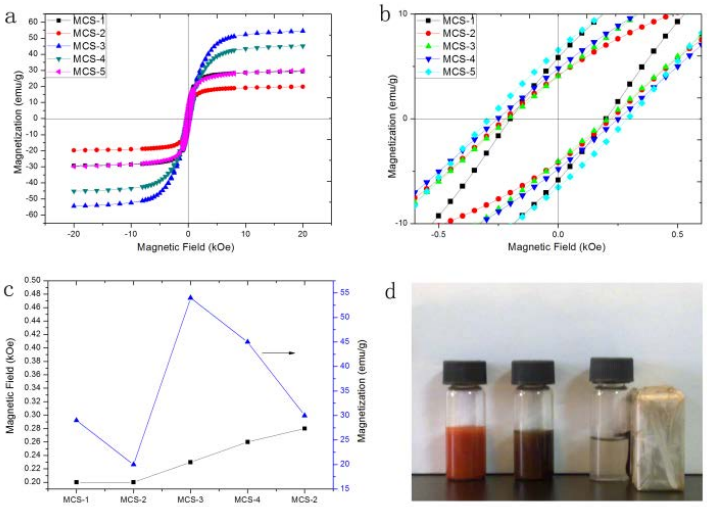

Figure 4 Hysteresis loop (a) of the Fe_3O_4@CuSilicate nanorattles measured at 300 K and the enlarged view (b) of the hysteresis loop between -600 Oe and 600 Oe,(c) demonstrates the saturation magnetization and coercivity of Fe_3O_4@CuSilicate with different aspect ratio and thicknesses of copper silicate shell, (d) shows photographic images of the α-Fe_2O_3@CuSilicate (left) and Fe_3O_4@CuSilicate nanorattles suspended in ethanol in the absence (middle) and presence (right) of an external magnet.

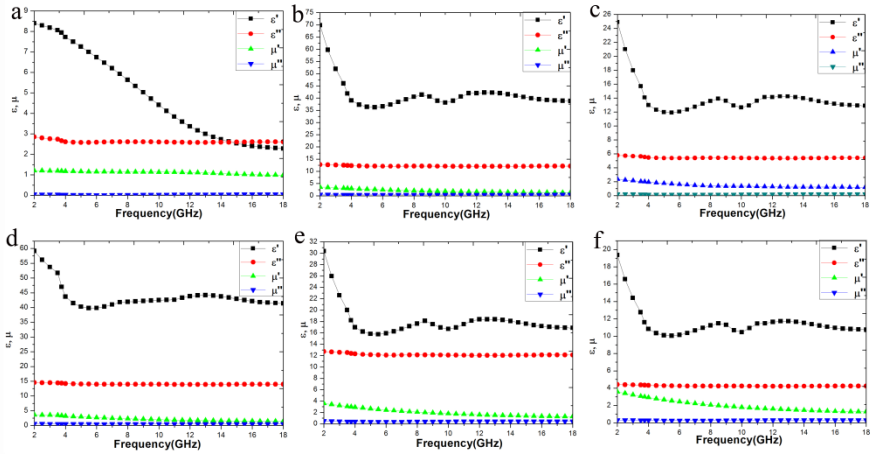

Figure 5 Frequency dependence of complex permittivity and permeability of the Fe_3O_4@CuSilicate nanorattles /EP composites: (a) RM, (b) MCS-1, (c) MCS-2, (d) MCS-3, (e) MCS-4, and (f) MCS-5.

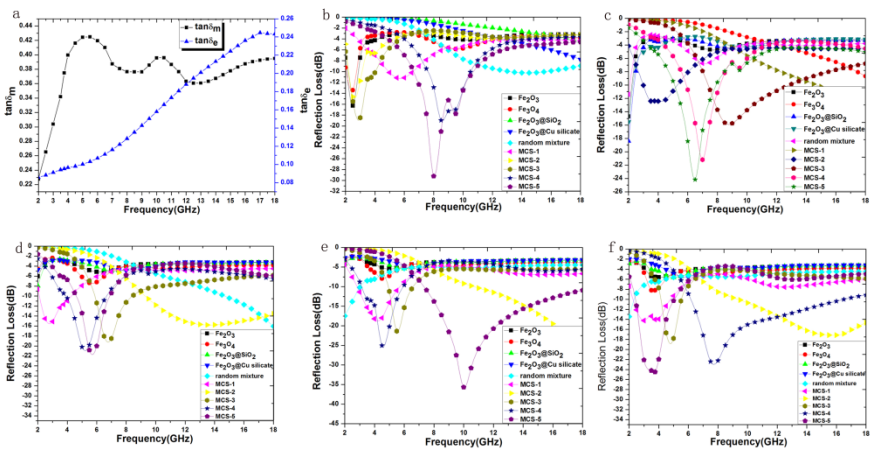

Figure 6 (a) Dielectric loss (tan $\delta_e = \varepsilon''/\varepsilon'$) and magnetic loss (tan $\delta_m = \mu''/\mu'$) of MCS-1, and microwave reflection loss curves of the α-Fe_2O_3/EP, α-Fe_2O_3@SiO_2/EP, α-Fe_2O_3@CuSilicate/EP, and Fe_3O_4@CuSilicate/EP composites at different thickness: (b) 2 mm, (c) 2.5 mm, (d) 3 mm, (e) 3.5 mm, (f) 4 mm.

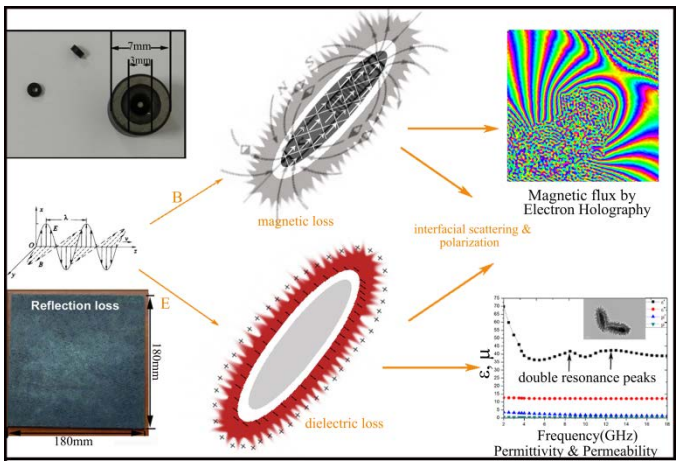

Figure 7 A schematic model of the microwave absorption mechanism of the as-made Fe_3O_4@CuSilicate